MedCrave
Step into the World of Research

Fluid Mechanics Research International Journal

Research Article

Open Access

CrossMark

Oblique frictional unilateral pounding analysis in two successive curved bridge (s type) segments

Abstract

Structures lying in close proximity experience multi-body dynamics, the impact phenomenon of which is known as pounding. This may lead to deck-unseating or in-plane deck rotation, phenomenon usually observed during high seismic activities. This leads to the important aspect of calculating the possibility of stick and slip to understand the safety of the design. The calculation is carried out by employing a linear complementarity in both the linear and tangential directions for observing the interaction between the two decks, which are considered to be rigid. The various conditions of the pre-impacting parameters, for all the possible stick-stick combinations, in the case of single impact are analytically determined. It is observed that the rotational potential of the deck, in-plane, is present for curved bridges having S-type configuration and needs to be considered while designing.

Keywords: multi-body dynamics, frictional impact, segmental curved bridges, linear complementarity problem, unilateral contact

Volume 1 Issue 2 - 2017

A Chanda,[1] A Banerjee,[2] Raj Das[3]

[1]Center for Advanced Composite Materials, The University of Auckland, New Zealand
[2]Department of Mechanical Engineering, The University of Auckland, New Zealand
[3]Sir Lawrence Wackett Aerospace Research Centre, RMIT University, Australia

Correspondence: Avishek Chanda, PhD Student, Center for Advanced Composite Materials, Department of Mechanical Engineering, The University of Auckland, 20 Symonds Street, 1010, Auckland, New Zealand, Tel +64226792780
Email acha553@aucklanduni.ac.nz

Received: July 03, 2017 | **Published:** October 02, 2017

Introduction

The most used life-line structure of the modern day is the bridges, which has been developed significantly, with the most recent introduction being of the curved bridges. They provide an aesthetic look and are also very convenient at various crossings and cross-over. However, curved bridges have been observed to have poor seismic response. Pounding between the adjacent segments, in-plane deck rotation and deck abutment interaction make the curved bridges very susceptible during such activities, resulting in deck unseating, shear failure, torsional failure and the interfacial concrete failure.[1]

San Fernando earthquake, in 1971, saw the first deck un-seating in the Golden state - Antelope Valley freeway interchange in California.[1,2] Many other devastations observed in the Loma Prieta earthquake, Northridge earthquake,[1,3] Chile earthquake,[4] Christchurch earthquake[5–7] and others brought out the necessity of making structures earthquake resistance, especially in the case of the curved bridges. The first experimental study, on curved bridges, was conducted in 2014 to observe and analysis the rotation of segmental curved bridges, the governing mechanics and the pounding failure patterns.[8,9] However, a proper thorough analytical analysis on the pounding of curved bridges is very limited; whereas, straight and skew bridges have a significant amount of studies in the current literature.[4,10–20] Therefore, analysing the impact behaviour of the S-oriented curved bridges is a first and this study aims to fill a very important gap in the literature.

Compliance method forms the usual method used for modelling pounding mechanisms, simulating the entire phenomenon with contact elements, such as, damped springs (Kelvin elements)[21–23] and non-linear springs (Hertz)[24–26] considering impact to be centric and allowing penetration during contact. Other significant studies include the two-dimensional study by Andreaus et al.,[27] SDOF oscillator without friction[28] and considering friction[29,30] and observing the forced motion of a oscillator, having friction, which is limited by both rigid an deformable bodies.[31] However, Chanda et al.,[32] & Banerjee et al.,[33]studied the behaviours of the various impact models and concluded that the unilateral contact is the most suited method in the field of non-smooth dynamics for calculating impact between two segments, because time-lag due to penetration will always take place in the case of compliance methods.[34–37] Moreau[38] & Panagiotopoulos[39,40] first applied this method in the impact analysis, by transforming the inequality forms of the laws of impact. Following comprehensive works by Abbas et al.[41] Glocker[42] and others helped in the usual personification of the ideas of convex study and laws in the method of unilateral contact. Further studies by Leine et al.,[43] on simulated toy structures, such as, woodpecker, the tumbling toy and the waddling duck, have helped in establishing the method firmly into the field of impact analysis. Subsequently, Theodosiou et al.,[44] analysed the dynamic response involved in multiple unilateral contacts in the large scale, using finite element approach. Dimitrakopoulus[10] then extended the work for observing the seismic behaviour experienced by skewed bridges, which is further extended in this study.

Newton's impact and Coulomb's frictional laws, are implemented to study the stick slip possibilities, due to the various pre-impact conditions, in curved bridges, in the normal and transverse directions respectively. The governing geometry greatly influences the post-impact deck responses, which is again dependent on the pre-impact conditions and this complex phenomenon is analytically studied for single impact conditions during deck-deck pounding of a curved bridge with two successive segments forming an S, both the decks being rigid. All the possible cases of slip and stick, when the two furthest points of each deck are in contact with the other's contour, are elucidated in Figure 1. The study helps to observe the safety conditions in constructing such bridges with future references for designers and analysists.

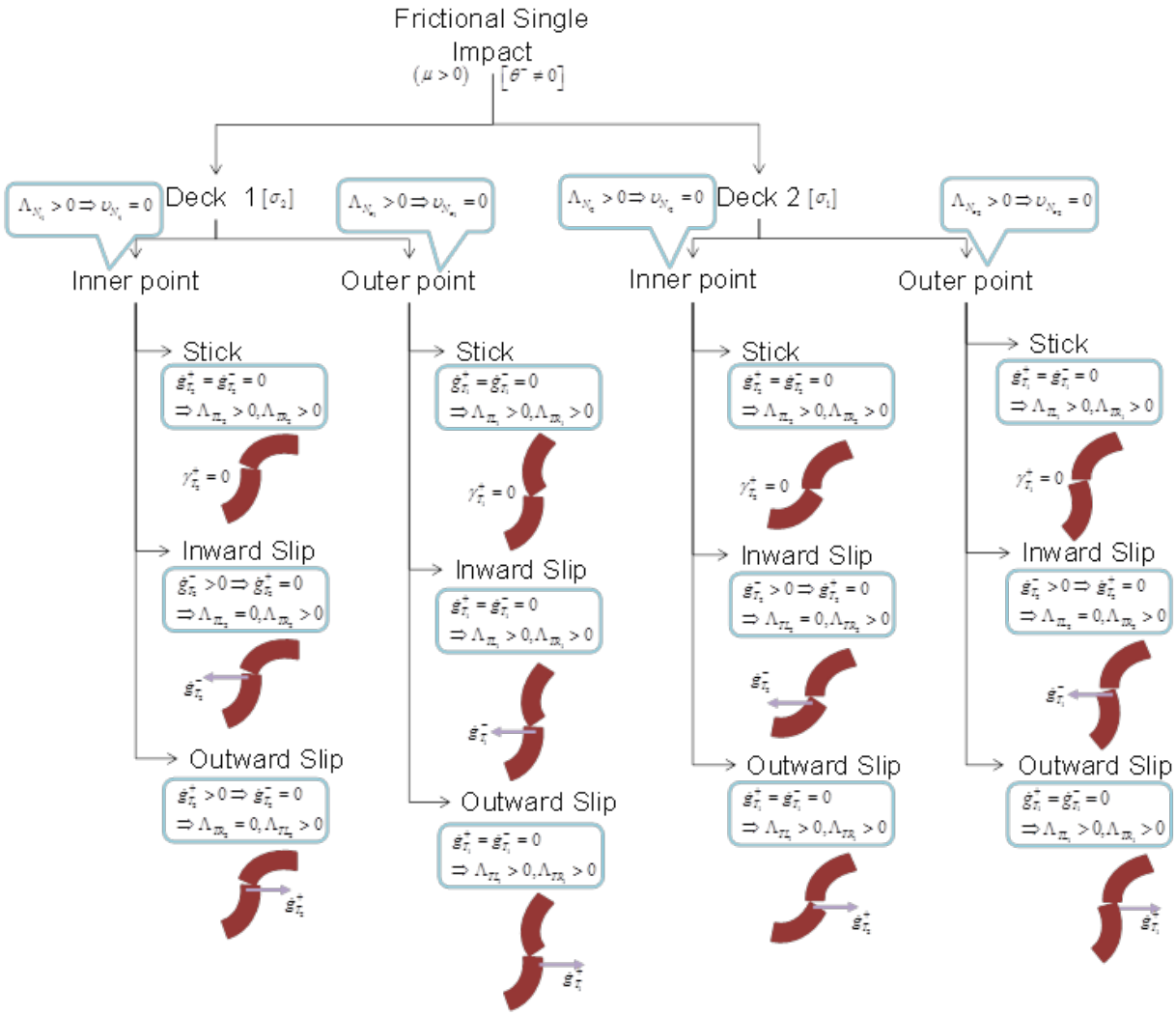

Figure 1 The classification of the entire frictional post-impact phenomenon.

Methodology and governing parameters

Oblique unilateral frictional contact method is based on the Newton's impact law along the normal direction and the Coulomb's frictional law in the transverse or oblique direction.[45,46] Therefore, the coefficient of friction (μ) and the coefficient of restitution (ε_N) constitute the two important parameters for simulating the frictional effect. Thus, the two laws are used to formulate a problem on the linear complementarity (LCP), which can depicted as $y = Ax + B$, in which A and B are the known quantities, with the constraint $y^T x = 0, \forall x, y \geq 0$, and representing that either x or y is zero or else positive. The LCP is solved using the Lemke's algorithm.[47,48] The ratio between the relative post-impact (γ_N^+) and pre-impact (γ_N^-) velocities is known as the coefficient of restitution (ε_N). It can be followed from the work of Banerjee et al.,[49] that based on these and using Newton's Impact Law and Coulomb's Frictional Law, with the range of the coefficient of restitution being $\varepsilon_N \in [0,1]$ and assuming $\varepsilon_T = 0$ in the oblique direction, the linear complementarity equation, in a coupled set, is represented as:

$$\begin{Bmatrix} \upsilon_N \\ \gamma_T^+ \\ \Lambda_{TL} \end{Bmatrix} = \begin{bmatrix} (G_{NN} - \mu G_{NT}) & G_{NT} & 0 \\ (G_{TN} - \mu G_{TT}) & G_{TT} & I \\ 2\mu & -I & 0 \end{bmatrix} \begin{Bmatrix} \Lambda_N \\ \Lambda_{TR} \\ \dot{g}_T^- \end{Bmatrix} + \begin{Bmatrix} (I + \varepsilon_N)\gamma_N^- \\ \gamma_T^- \\ 0 \end{Bmatrix} \tag{1}$$

where, Λ is the impulse, υ_N is the velocity jump, $\gamma_T^{\pm}$ is the relative velocity at post and pre-impact conditions in the transverse direction and G_{xx} represents the effective mass for different conditions. Various states of impact, such as 'stick' and 'slip', for single impact as well as double impact, can be evaluated using the LCP formulation, illustrated in Eq. (1). The biggest advantage of the LCP method is

Citation: Chanda A, Banerjee A, Das R. Oblique frictional unilateral pounding analysis in two successive curved bridge (s type) segments. *Fluid Mech Res Int.* 2017;1(2):33–43. DOI: 10.15406/fmrij.2017.01.00006

the availability of all the elements in the form of matrices, instead of being in scalar quantities, as found in the Compliance Method. It should be noted that j represents the number of the deck $(1,2)$ and k represents the inner or outer point (i,o) of each deck. The widths of the decks (W) are also considered to be equal and constant and so are the thicknesses (t).

Determination of the governing parameters

The post-impact behaviour of the bridge segment is dependent mainly on the effective mass of impact (G_{NN}) and the mass matrix (M). The other dependent parameters are estimated based on the pre-impact conditions and the different impacting orientations of the deck segment as illustrated in Figure 2. The decks are in contact at the lower parts of each and thus, only the distances of the lever arms are considered for the lower part of each. The considerable distances, the plan area, the centre of masses and the moments of inertia are calculated based on the similar formulations thoroughly elucidated in the work presented by Banerjee et al.[49] Therefore, the mass matrix is calculated to be:

$$M=diag\left\{m_1 \quad m_1 \quad I_{m_1} \quad m_2 \quad m_2 \quad I_{m_2}\right\} \tag{2}$$

The lever arms are also calculated based on the same formulation for both the conditions of decks not rotating and the decks rotating about the centre of mass.

Therefore, considering the rigid body rotation, the value of the lever arms change to:

$$\begin{aligned}
\tilde{r}_{N_{i_j}} &= r_{N_{i_j}} \cos\theta_j + r_{T_{i_j}} \sin\theta_j \\
\tilde{r}_{N_{o_j}} &= r_{N_{o_j}} \cos\theta_j + r_{T_{o_j}} \sin\theta_j \\
\tilde{r}_{T_{i_1}} &= -r_{N_{i_1}} \sin\theta_1 + r_{T_{i_1}} \cos\theta_1 \\
\tilde{r}_{T_{o_1}} &= -r_{N_{o_1}} \sin\theta_1 + r_{T_{o_1}} \cos\theta_1 \\
\tilde{r}_{T_{i_2}} &= r_{N_{i_2}} \sin\theta_2 - r_{T_{i_2}} \cos\theta_2 \\
\tilde{r}_{T_{o_2}} &= r_{N_{o_2}} \sin\theta_2 - r_{T_{o_2}} \cos\theta_2
\end{aligned} \tag{3}$$

where, $\tilde{r}_{N_{i_j}}$ & $\tilde{r}_{N_{o_j}}$ $(j=1,2)$ represent the distance from the centre of mass of the normal drawn on the inner and outer potential impacting points of the decks and $\tilde{r}_{T_{i_j}}$ & $\tilde{r}_{T_{o_j}}$ denote that of the transverse drawn on the same points.

The direction matrices for the two decks due to rotation by θ_1 & θ_2 angles respectively are derived and the normal and tangential distances of the centre of mass are deduced as:

$$\begin{Bmatrix} \tilde{r}_{N_{\theta_{k_j}}} \\ \tilde{r}_{T_{\theta_{k_j}}} \end{Bmatrix} = \begin{bmatrix} \cos\theta_j & -\sin\theta_j \\ \sin\theta_j & \cos\theta_j \end{bmatrix} \begin{Bmatrix} \tilde{r}_{N_{k_j}} \\ \tilde{r}_{T_{k_j}} \end{Bmatrix} \tag{4}$$

where, $\hat{j}$ is complementary to j, which means $j=1 \rightarrow \hat{j}=2$ and vice versa. The direction matrix helps to calculate the relation between the relative velocities between the two points of impact, with respect to the relative velocities between the two decks.

Therefore, the normal (W_{N_1}) and transverse (W_{T_1}) directional matrices, when deck-1 is in impact at the contour (σ_2) of deck-2 are:

$$\begin{aligned}
W_{N_{k_1}} &= \left\{-\sin\theta_2 \quad \cos\theta_2 \quad \tilde{r}_{N_{\theta_{2_{k_1}}}} \quad \sin\theta_2 \quad -\cos\theta_2 \quad \tilde{r}_{N_{\sigma_2}}\right\}^T \\
W_{T_{k_1}} &= \left\{\cos\theta_2 \quad \sin\theta_2 \quad \tilde{r}_{T_{\theta_{2_{k_1}}}} \quad -\cos\theta_2 \quad -\sin\theta_2 \quad \tilde{r}_{T_{\sigma_2}}\right\}^T
\end{aligned} \tag{5}$$

In the same way, the direction matrices when deck-2 is in impact with that of the contour (σ_1) of deck-1 are:

$$\begin{aligned}
W_{N_{k_2}} &= \left\{-\sin\theta_1 \quad \cos\theta_1 \quad \tilde{r}_{N_{\sigma_1}} \quad \sin\theta_1 \quad -\cos\theta_1 \quad \tilde{r}_{N_{\theta_{1_{k_2}}}}\right\}^T \\
W_{T_{k_2}} &= \left\{\cos\theta_1 \quad \sin\theta_1 \quad \tilde{r}_{T_{\sigma_1}} \quad -\cos\theta_1 \quad -\sin\theta_1 \quad \tilde{r}_{T_{\theta_{1_{k_2}}}}\right\}\theta_1^T
\end{aligned} \tag{6}$$

In Eqs. (5) and (6), the respective directional distances of the impacting points from the centre of masses are represented as $\tilde{r}_{N_{\sigma_1}}$ & $\tilde{r}_{T_{\sigma_1}}$ and $\tilde{r}_{N_{\sigma_2}}$ & $\tilde{r}_{T_{\sigma_2}}$ respectively.

Similarly, following the work done by Banerjee et al.,[49] on single segment curved bridges, the distance vector, r_D, is calculated as:

$$r_D = \begin{pmatrix} r_{N_{i_2}} - r_{N_{i_1}} + x_2 - x_1 + \tilde{r}_{N_{\sigma_1}} - \tilde{r}_{N_{\sigma_2}} \\ Y_{m_1} + Y_{m_2} + g - \tilde{r}_{T_{\sigma_1}} - \tilde{r}_{T_{\sigma_2}} + y_1 - y_2 \\ 0 \end{pmatrix} \tag{7}$$

Therefore, with respect to the contours of impact, the normal and tangential coefficients of the distance vector, after the decks rotated by θ_1 & θ_2 respectively, are:

$$\begin{aligned}
n_1 &= \begin{pmatrix} \sin\theta_1 \\ -\cos\theta_1 \\ 0 \end{pmatrix} \& \; t_1 = \begin{pmatrix} \cos\theta_1 \\ \sin\theta_1 \\ 0 \end{pmatrix} \\
n_2 &= \begin{pmatrix} -\sin\theta_2 \\ \cos\theta_2 \\ 0 \end{pmatrix} \& \; t_2 = \begin{pmatrix} -\cos\theta_2 \\ -\sin\theta_2 \\ 0 \end{pmatrix}
\end{aligned} \tag{8}$$

The respective impact points are thus calculated by considering the two instances separately. The first instance is the inner and outer edges of the deck-2 interacting with σ_1, an unknown point on contour of deck-1, and the second being the exact thing occurring for deck-1. The unknown points are calculated as:

$$\begin{aligned}
\sigma_1 = R_1 - X_{m_1} + \left(R_2 + \sigma_2 - X_{m_2}\right)\cos\left(\theta_1 - \theta_2\right) - Y_{m_2} \sin\left(\theta_1 + \theta_2\right) + \\
\left(r_{N_{i_2}} - r_{N_{i_1}} + x_2 - x_1\right)\cos\theta_1 + \left(Y_{m_1} + Y_{m_2} + g + y_1 - y_2\right)\sin\theta_1
\end{aligned} \tag{9}$$

Citation: Chanda A, Banerjee A, Das R. Oblique frictional unilateral pounding analysis in two successive curved bridge (s type) segments. *Fluid Mech Res Int.* 2017;1(2):33–43. DOI: 10.15406/fmrij.2017.01.00006

Similarly, it is also derived that:

$$\sigma_2 = -R_2 + X_{m_2} + \left(R_1+\sigma_1-X_{m_1}\right)\cos\left(\theta_1-\theta_2\right) + Y_{m_1}\sin\left(\theta_1-\theta_2\right) - 2Y_{m_2}\sin\theta_2\cos\theta_2 + \left(r_{N_{i_2}} - r_{N_{i_1}} + x_2 - x_1\right)\cos\theta_2 + \left(Y_{m_1}+Y_{m_2}+g+y_1-y_2\right)\sin\theta_2 \tag{10}$$

The exact values of $\sigma_1 \& \sigma_2$ is calculated from the Eqs. (9) and (10) by considering:

$$-W/2 \leq \sigma_{\hat{j}} \leq W/2 \tag{11}$$

The value of $\sigma_{\hat{j}} = -W/2$ is considered when the inner point of deck-2 is in contact and $\sigma_{\hat{j}} = W/2$ when the impact occurs on the outer point.

The gap, when deck-2 is in impact, is calculated from the vector equation, $r_D^T n_j = g_{N_j}$, as:

$$g = 2\sigma_1\tan\theta_1 + \left(r_{N_{i_2}} - r_{N_{i_1}} + x_2 - x_1\right)\tan\theta_1 + \frac{Y_{m_1}}{\cos\theta_1} - \left(R_2+\sigma_2-X_{m_2}\right)\left(\tan\theta_1\cos\theta_2-\sin\theta_2\right) + Y_{m_2}\left(\cos\theta_2-\tan\theta_1\sin\theta_2\right) - \left(Y_{m_1}+Y_{m_2}+y_1-y_2\right) \tag{12}$$

On the contrary, the gap, when deck-1 is in impact, is also calculated as:

$$g = 2\sigma_1\tan\theta_2 + \left(r_{N_{i_2}} - r_{N_{i_1}} + x_2 - x_1\right)\tan\theta_2 + \left(R_1-\sigma_1-X_{m_1}\right)\left(\tan\theta_2\cos\theta_1-\sin\theta_1\right) - Y_{m_1}\left(\cos\theta_1+\sin\theta_1\tan\theta_2\right) - Y_{m_2}\left(\tan\theta_2\sin\theta_2-\cos\theta_2\right) - \left(Y_{m_1}+Y_{m_2}+y_1-y_2\right) \tag{13}$$

Results and discussion

The possible impacting points can be observed from Figure 2, only considering in-plane deck-rotation. The stick-slip calculations are carried out with respect to the coordinate system of deck-2. The various conditions, during impact, as illustrated in Figure 1, are used to calculate the ratio between the pre-impact velocities, the most important pre-impact parameter to be considered by the designers during the design phase. The stick-slip occurrence, at the instance of impact, is significantly affected by the ratio of oblique and normal pre-impact velocities $\left(\gamma_T^- / \gamma_N^-\right)$ and by the geometrical parameters of the deck, such as, the decks' curved angles $\left(\beta_1 \& \beta_2\right)$, the radii of the two decks $\left(R_1 \& R_2\right)$ and the angles of rotation $\left(\theta_1 \& \theta_2\right)$ experienced by the decks. Thus, the pre-impact velocities are calculated, based on the directional matrices calculated from Eqs. (2,5,6) for each case of single impact, following the same trend as presented in the work presented by Banerjee et al.[49] It is observed that, the variation of the entire phenomenon of single impact is based on a single parameter, coined ∂ , with the width (W) of both the decks being 10 meters. The entire parametric analysis is carried out based on the variations in the values of the curve angles $\left(60^\circ, 90^\circ, 120^\circ\right)$, radii of each bridge (100 meters and 200 meters), values of the coefficient of friction (0.5 and 1) and the value of the coefficient of restitution in the normal direction (ε_N) being 0.5 for all the cases.

The phenomenon, when one of the four potential impacting points comes into contact with the surface of the other deck at σ_j , is known as single impact. This occurs due to the pre-impact angular velocity experienced due to the deck rotation. When frictional impact is considered, the body starts slipping, when the resisting frictional force is surpassed, which may result in the un-seating of the deck due to the amplified in-plane deck rotation. Graphs are plotted based on the pre-impact velocity ratios observed for each case.

The parametric analysis, illustrated in Figures 3–6, is conducted on the curved deck geometries for different curved angles of 60^0 and 90^0 for the two decks, each having two radii of 100meters and 200meters. (Figure 3) (Figure 4) represent how the variation in sticking and slipping regions take place for 2 sets of β values when both the inner and outer points are in contact with the surface of the other deck. The increase in stick region is obvious with the increase in the coefficient of friction, as more force is required to overcome it. When deck-2 is in impact with the contour of deck-1, the stick region gradually increases for both inward and outward slip, when the inner point is in contact; whereas, an opposite trend is observed when the outer point is in contact.

A unique feature is observed at the instance of deck-1 hitting deck-2, when the radius of deck-1 is 200m and that of deck-2 is 100m, where the amount stick region is more when the inner point of deck-1 is in contact and gradually decreases when the outer point is in impact.

Figures 5 & 6 elucidates that the variation in sticking and slipping regions for 2 other sets of β values respectively, when either the inner or the outer points are in impact. The variation between the deck-1 hitting the surface of deck-2 and deck-2 hitting the surface of deck-1 are shown and it can again be observed that the increase in friction also results in the increase of the sticking region.

Maximum linear stick is again observed when the deck-1 is in contact with the contour of deck-2 and the frictional coefficient is 0.5. Variations in the stick regions can be observed with the amount of stick region being more when the inner point of deck-2 is in contact with the contour of deck-1.

The upper and lower planes, in Figures 3–6 represent the region of sticking with varying ratios of tangential and normal post-impact velocities in the z-axis, pre-impact rotation of deck-2 along the y-axis and that of deck-1 along the x-axis. -10 to 10 is considered to be the range of rotation of both the decks; whereas, -12 to 12 is taken in the range of γ_T^- / γ_N^- . The portions in graphs, above and below the sticking region, represent the various slipping conditions, namely, the inner point inward and outward slip and the outer point inward and outward slip for each deck.

These conditions are classified based on the thorough analytical

concepts elaborated in the previous sections. The classification of the stick and slip regions, as represented by the graphs provided for studying the phenomenon of single impact, are explained in details in Figures 7 & 8.

The regions of inward and outward slip along with the representation of the specific point of impact, when the inner or outer point of deck-1 is in impact with the contour of deck-2, are elucidated in Figure 7. The inner-point impact occurs when deck-2 rotates in the positive direction; whereas, the impact is experienced at the outer point when deck-1 rotates in the positive direction. An opposite trend in the direction of inner point impact and outer point impact can be observed when single impact phenomenon is experienced by deck-2 on the contour of deck-1. The impact on the inner point is experienced when deck-1 rotates in the positive direction and that on the outer point is experienced when deck-2 rotates in the positive direction, the graphical representation of which is given in Figure 8.

It is known that the value of $\gamma_{N_{k_j}}^{-}$ is always negative and for the existence of outward slip the value of $\gamma_{T_{k_j}}^{-}$ should be positive. Thus, the ratio between $\gamma_{T_{k_j}}^{-} \Big/ \gamma_{N_{k_j}}^{-}$ is always negative (<0) and therefore the direction of the outward slip is represented by the lower part (negative region) of the $\gamma_T^{-} \Big/ \gamma_N^{-}$ axis, for both the cases. Similarly, the value of $\gamma_{T_{k_j}}^{-}$ is always negative which results in the representation of the inward slip on the upper part (positive side) of the $\gamma_T^{-} \Big/ \gamma_N^{-}$ axis. A comparatively linear variation, between the outward and inward slip, for both inner and outer point impacts is observed for all the cases, when the radii of both the decks are equal. The post-impact phenomenon is predictable and no abrupt variation is observed when the decks have equal radii, thus making the designs relatively convenient and safer. With $R_1 > R_2$, the region of sticking is observed to be higher when the inner point of deck-1 is in contact with the contour of deck-2, when the inner point of deck-2 is in contact with the contour of deck-1 and the coefficient of friction is 0.5 and when the outer point of deck-2 experiences impact with the contour of deck-1 and the coefficient of friction is 1.

On the other hand, with $R_1 < R_2$, the amount of stick is linear for both the points of impact when deck-1 experiences contact with deck-2 and the coefficient of friction is 0.5 and the region of stick is higher when the outer point of deck-1 hits deck-2 and the coefficient of friction is 1 and when the inner point of deck-2 hits deck-1 with both the coefficients of friction. Moreover, the tendency of outward slip is observed to be higher in general when deck-1 is in contact with deck-2 for all the variations of the radii; although, quite a few cases, with the coefficient of friction being unity, have almost proportional amount of outward and inward slip. In the case of the impacting points of deck-2 coming in contact with the contour of deck-1, the tendency of outward slip is higher at the instance of the outer point being in contact and that of the inward slip is higher at the instance of the inner point being in contact, when $R_1 < R_2$ and also when $R_1 > R_2$ and the coefficient of friction is 1. On the contrary, when the coefficient of friction is 0.5 and $R_1 > R_2$ the tendency of inward slip is higher at the instance of the outer point of deck-2 being in contact with the contour of deck-1 and the outward slip is more when the inner point of deck-2 is in contact. The frictionless cases will be accompanied by only outward and inward slip, with a single demarcating plane along the axis, for describing the regions of the two slips (Table 1).

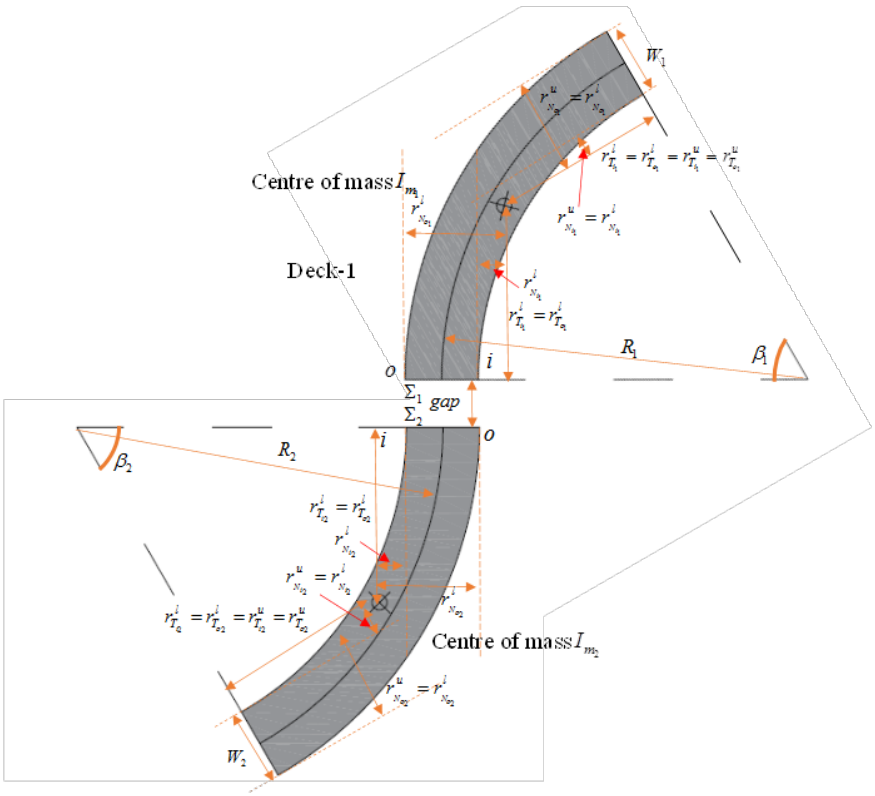

Figure 2 Deck geometry of the curved bridge showing the position of center of mass and the different impacting parameters without in-plane deck rotation.

Citation: Chanda A, Banerjee A, Das R. Oblique frictional unilateral pounding analysis in two successive curved bridge (s type) segments. *Fluid Mech Res Int.* 2017;1(2):33–43. DOI: 10.15406/fmrij.2017.01.00006

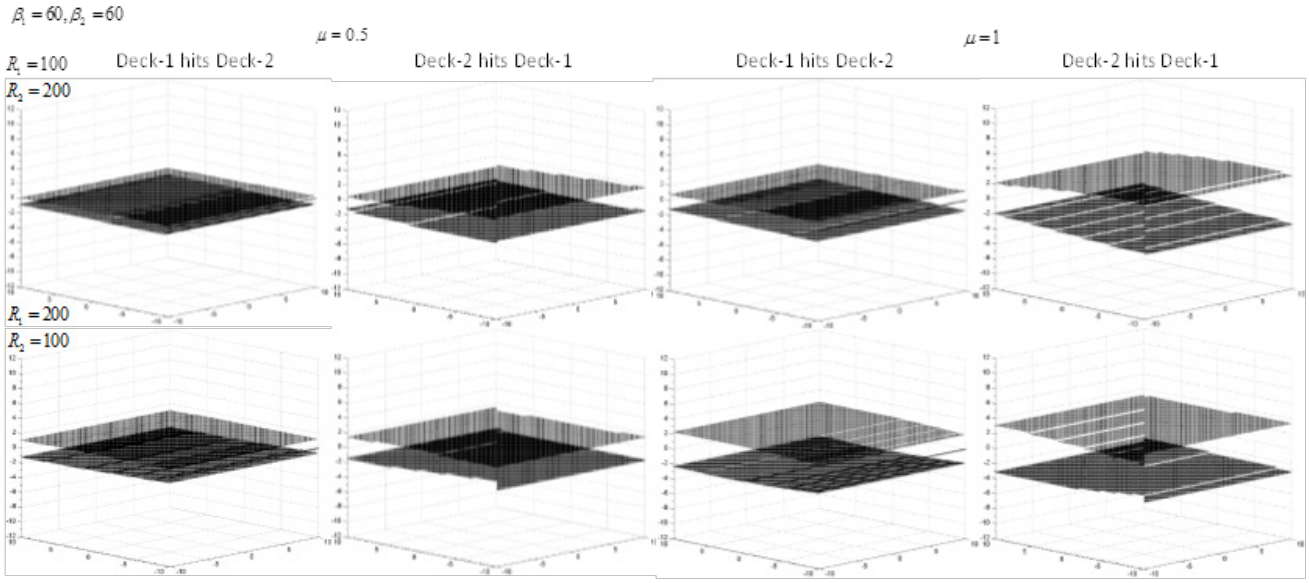

Figure 3 Illustration of the parametric study of the curved decks having 2 sets of values and with $\beta_1 = \beta_2 = 60^\circ$, when compared between the two cases of impact, namely, deck-1 is in impact with deck-2 and vice-versa, for different coefficients of friction.

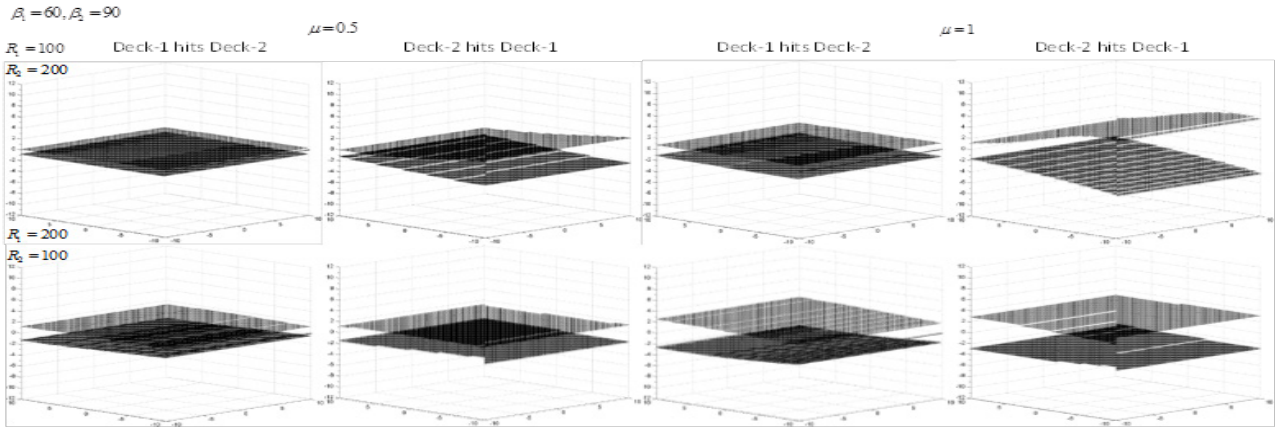

Figure 4 Illustration of the parametric study of the curved decks having 2 sets of values and with $\beta_1 = 60^0$ & $\beta_2 = 90^0$, between the two cases of impact, namely, deck-1 is in impact with deck-2 and vice-versa, for different coefficients of friction.

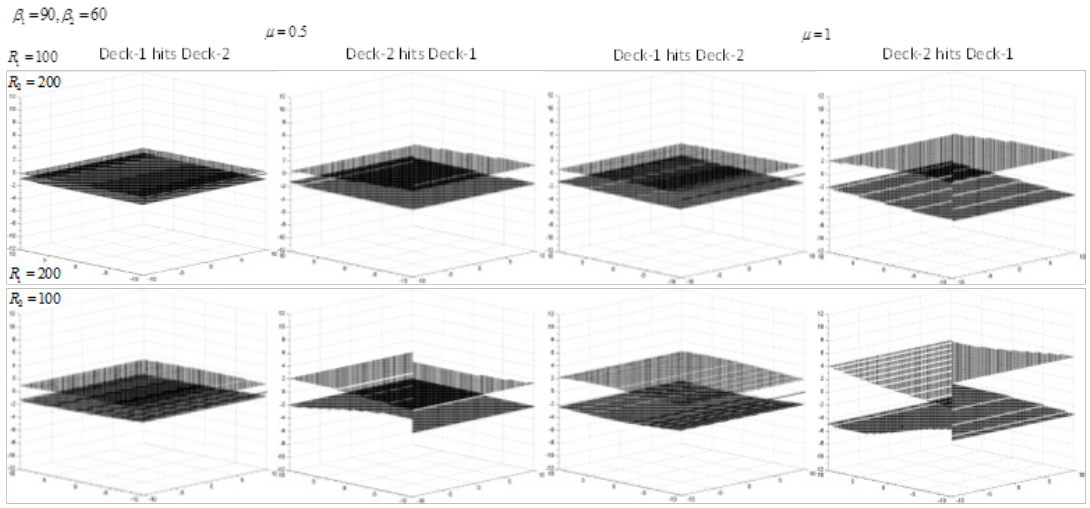

Figure 5 Illustration of the parametric study of the curved decks having 2 sets of R_j values and with $\beta_1 = 90^0$ & $\beta_2 = 60^0$, between the two cases of impact, namely, deck-1 is in impact with deck-2 and vice-versa, for different coefficients of friction.

Citation: Chanda A, Banerjee A, Das R. Oblique frictional unilateral pounding analysis in two successive curved bridge (s type) segments. *Fluid Mech Res Int.* 2017;1(2):33–43. DOI: 10.15406/fmrij.2017.01.00006

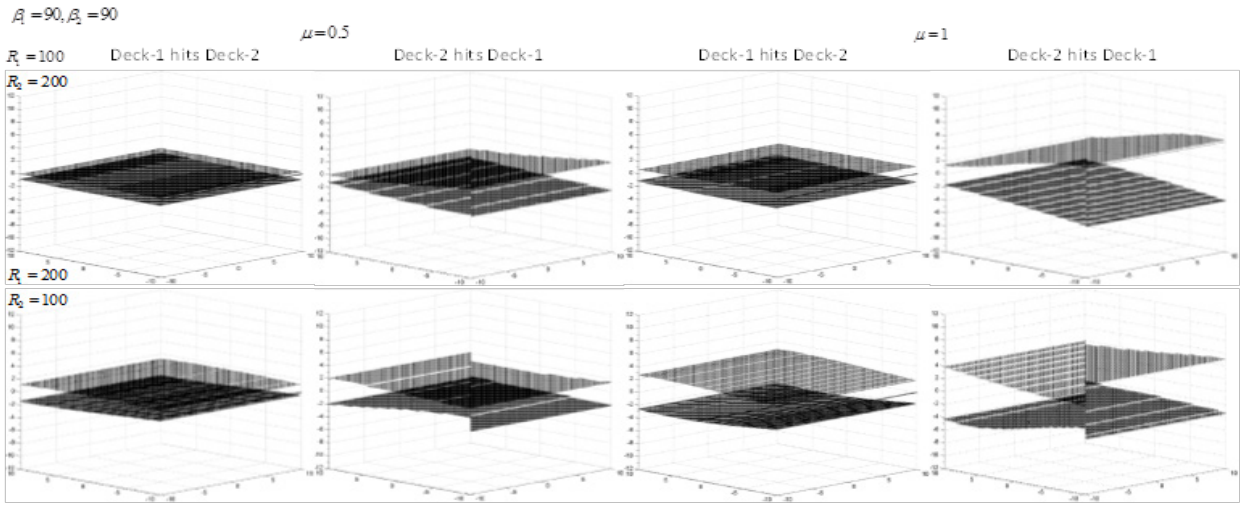

Figure 6 Illustration of the parametric study of the curved decks having 2 sets of R_j values and with $\beta_1=90^0 \& \beta_2=90^0$, between the two cases of impact, namely, deck-1 is in impact with deck-2 and vice-versa, for different coefficients of friction.

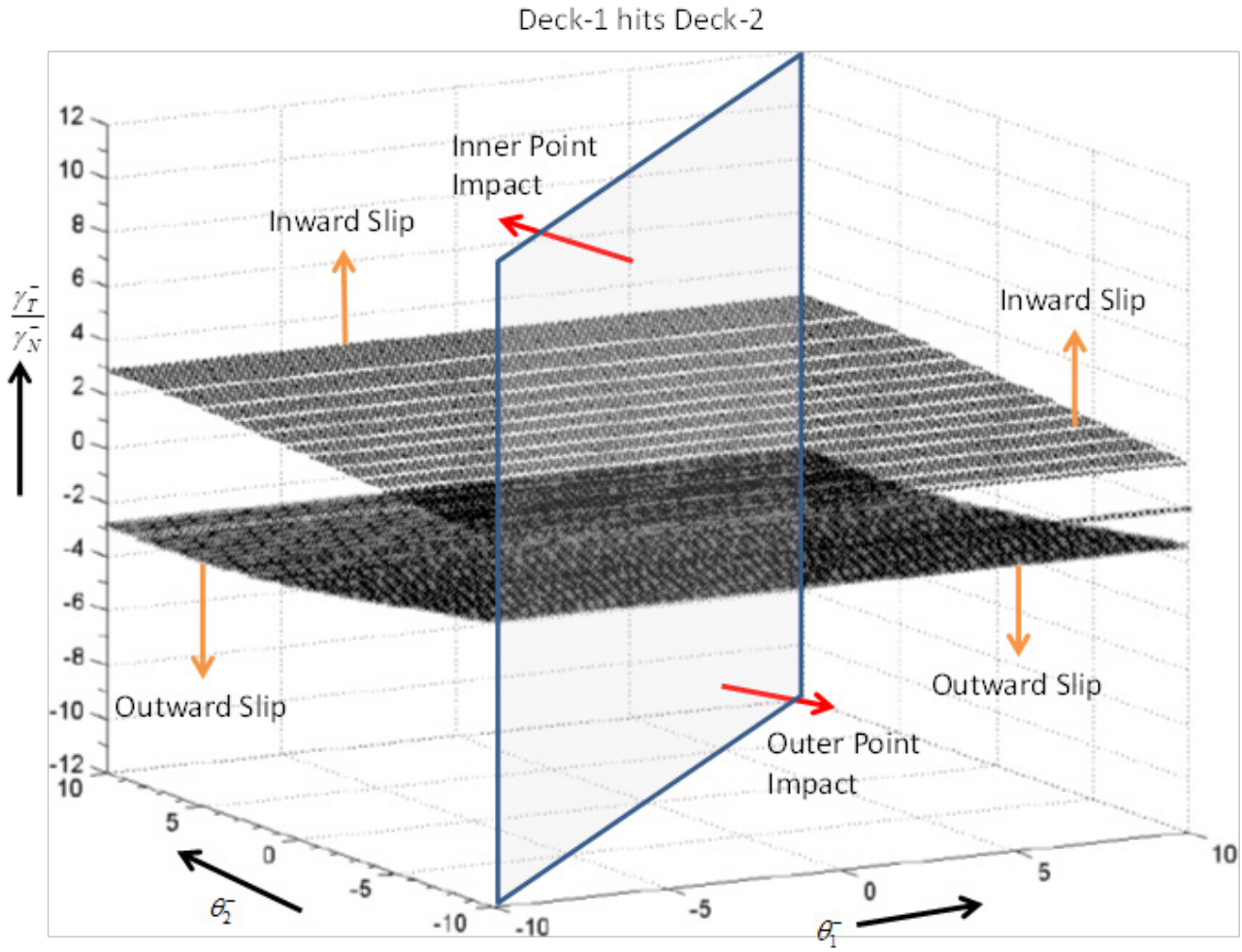

Figure 7 The different post-impact phenomenon, depicted by the graphs when both the inner and outer points of deck-1 is in contact with the contour of deck-2, during single impact.

Citation: Chanda A, Banerjee A, Das R. Oblique frictional unilateral pounding analysis in two successive curved bridge (s type) segments. *Fluid Mech Res Int.* 2017;1(2):33–43. DOI: 10.15406/fmrij.2017.01.00006

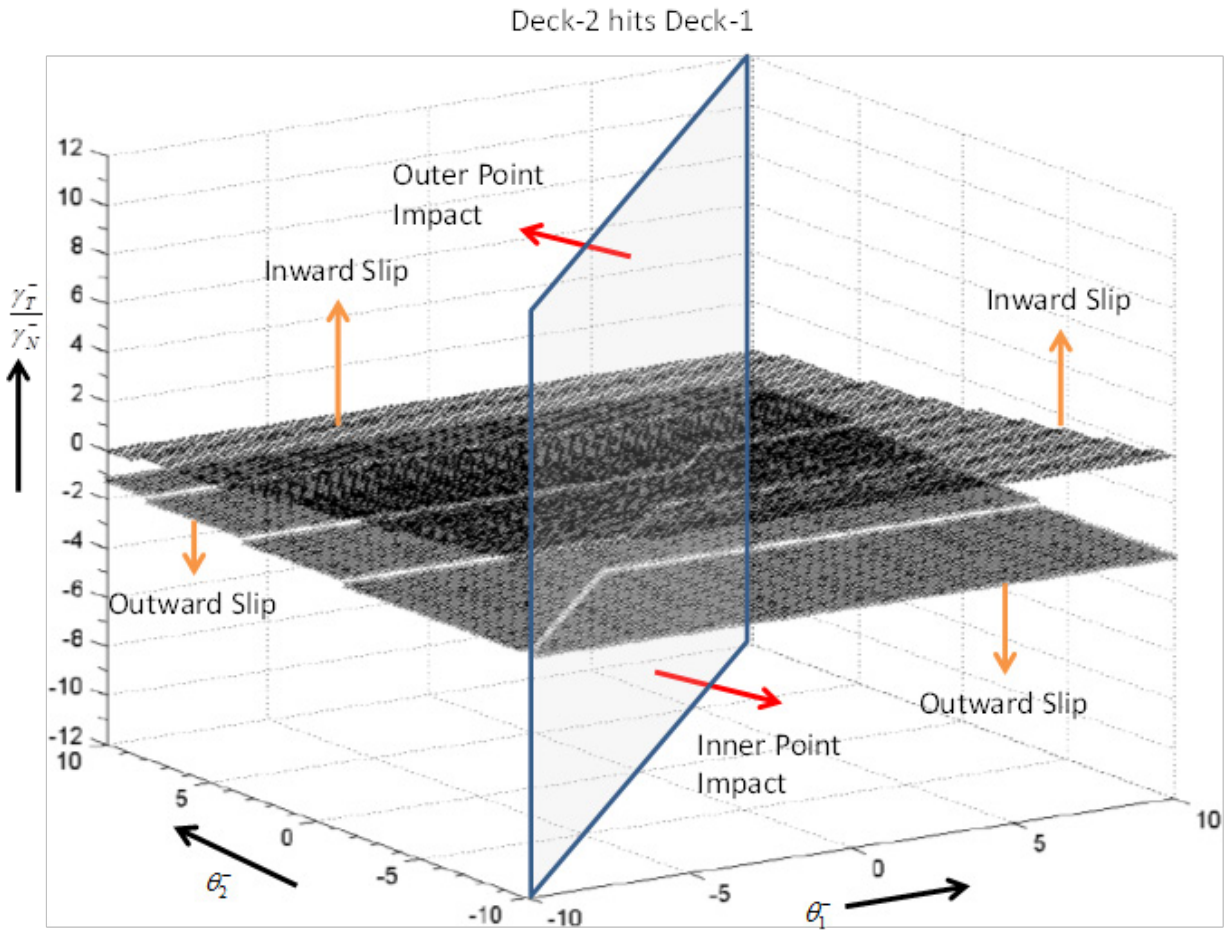

Figure 8 The different post-impact phenomenon, depicted by the graphs when both the inner and outer points of deck-2 is in contact with the contour of deck-1, during single impact.

Table 1 List of notations

Notations	Explanation
μ	Coefficient of friction
ε	Coefficient of restitution
LCP	Linear Complementarity Problem
A and B	Known quantities in the general form of LCP
$\gamma_Z^{\pm}$	Relative directional pre and post-impact velocities (Z=N,T; +=Post-impact; -=Pre-impact)
Λ_Z	Impulse in normal and tangential directions
υ_N	Velocity jump

Citation: Chanda A, Banerjee A, Das R. Oblique frictional unilateral pounding analysis in two successive curved bridge (s type) segments. *Fluid Mech Res Int.* 2017;1(2):33–43. DOI: 10.15406/fmrij.2017.01.00006

Table Continued

Notations	Explanation
G_{ZZ}	Effective mass
M	Mass matrix
I	Moment of inertia
mj	Mass of the decks (j=1,2)
i	Inner point of the deck
o	Outer point of the deck
$r_{Z_{l_j}}$	Distance of the lever arm (l=i, o)
θ	Angle of rotation of each deck
$\tilde{r}_{Z_{l_j}}$	Distance of the lever arm due to rotation
W_{Z_j}	Directional mass matrices
rD	Distance vector for the lever arm
g	Gap between the two decks
x_j & y_j	Distances
n_j & t_j	Directional coefficient of the distance vector
σ_1	Point on the contour of deck-1 where deck-2 is in impact
σ_2	Point on the contour of deck-2 where deck-1 is in impact
Rj	Radius of curvature of the two decks
$\overline{X}_{m_j}, \overline{Y}_{m_j}$	Center of masses of each deck
β_j	Curvature of the decks (600 and 900)
W	Width

Conclusions

Curved bridges with two successive rigid abutments, with S-type orientation, and their post-impact effects due to in-deck rotation are investigated in the present work. The rotational mechanics involved in the in-deck interaction, for curved bridges, have not been theoretically studied in the past and this paper illustrates a thorough non-smooth event based parametric analysis for identifying the possibility of stick and slip, after impact. The post-impact rotational potential is observed to depend on the total angle of the curve, the ratio of the pre-impact relative velocities in the tangential and normal directions and the coefficient of friction. Specifically, the post-impact slip and stick phenomenon, during single impact, in dependent entirely on the value of ∂ and the main focus of the designers should lie on this and its related parameters. The validity of inward slip is negligible when the coefficient of friction is greater than 0.25. Thus, it can be inferred

that the slipping tendency of curved bridges, during single impact, is considerably high and is an aspect which needs to be reduced in order to increase the safety of the structure.

Acknowledgments

None.

Conflicts of interest

Author declares that there is no conflict of interest.

References

1. Yashinsky M, M Karshenas. Fundamentals of seismic protection for bridges. *National Information Centre of Earthquake Engineering*. India. 2003. 184 p.
2. Jennings PC. Engineering features of the San Fernando earthquake of February 9, 1971. *Earthquake Engineering Research Laboratory*. 1971. 515 p.
3. Priestley MJN, Seible F, GM Calvi. *Seismic design and retrofit of bridges.* USA: John Wiley & Sons; 1996. 704 p.
4. Elnashai AS, Bora Gencturk, Oh Sung Kwonc, et al. The Maule (Chile) earthquake of February 27, 2010: Development of hazard, site specific ground motions and back-analysis of structures. *Soil Dynamics and Earthquake Engineering*. 2012;42:229–245.
5. Chouw N, H Hao. Pounding damage to buildings and bridges in the 22 February 2011 Christchurch earthquake. *International Journal of Protective Structures*. 2012;3(2):123–140.
6. Cole G, Rajesh Dhakal, Athol Carr, et al. Interbuilding pounding damage observed in the 2010 Darfield earthquake. *Bulletin of the New Zealand Society for Earthquake Engineering.* 2010;43(4):1–5.
7. Cole GL, RP Dhakal, FM Turner. Building pounding damage observed in the 2011 Christchurch earthquake. *Earthquake Engineering & Structural Dynamics*. 2012;41(5):893–913.
8. Wieser J, Arash E Zaghi, Manos Maragakis, et al. A methodology for the experimental evaluation of seismic pounding at seat-type abutments of horizontally curved bridges. *Structures Congress*. 2012;10:613–624.
9. Saad A, DH Sanders, I Buckle. Impact of Rocking Foundations on Horizontally Curved Bridge Systems Subjected to Seismic Loading. *Structures Congress*. 2012;10:625–635.
10. Dimitrakopoulos EG. Analysis of a frictional oblique impact observed in skew bridges. *Nonlinear Dynamics.* 2010;60(4):575–595.
11. Dimitrakopoulos EG. Non smooth analysis of the impact between successive skew bridge-segments. *Nonlinear Dynamics.* 2013;74(4):911–928.
12. Kim S. GIS-based regional risk analysis approach for bridges against earthquakes. Dissertation, Department of Civil Engineering, State University of New York, USA; 1993.
13. Maleki S. Seismic Modeling of Skewed Bridges with Elastomeric Bearings and Side Retainers. *Journal of Bridge Engineering*. 2005;10(4):442–449.
14. Maragakis EA, PC Jennings. Analytical models for the rigid body motions of skew bridges. *Earthquake Engineering & Structural Dynamics*. 1987;15(8):923–944.
15. Zhu P, M Abe, Y Fujino. Modelling three-dimensional non-linear seismic performance of elevated bridges with emphasis on pounding of girders. *Earthquake engineering & structural dynamics*. 2002;31(11):1891–1913.
16. Saadeghvaziri MA, A Yazdani Motlagh. Seismic behavior and capacity/demand analyses of three multi-span simply supported bridges. *Engineering Structures*. 2008;30(1):54–66.
17. Kaviani P, F Zareian, E Taciroglu. Seismic behavior of reinforced concrete bridges with skew-angled seat-type abutments. *Engineering Structures*. 2012;45:137–150.
18. Kawashima K, G Shoji. Effect of restrainers to mitigate pounding between adjacent decks subjected to a strong ground motion. *Proceeding of the 12th World Conference on Earthquake Engineering.* 2000.
19. Kawashima K, Tirasit P. Effect of nonlinear seismic torsion on the performance of skewed bridge piers. *Journal of Earthquake Engineering*. 2008;12(6):980–998.
20. Banerjee S, M Shinozuka. Nonlinear Static Procedure for Seismic Vulnerability Assessment of Bridges. *Computer-Aided Civil and Infrastructure Engineering*. 2007;22(4):293–305.
21. Anagnostopoulos SA. Pounding of buildings in series during earthquakes. *Earthquake Engineering & Structural Dynamics.* 1988;16(3):443–456.
22. Anagnostopoulos SA, KV Spiliopoulos. An investigation of earthquake induced pounding between adjacent buildings. *Earthquake engineering & structural dynamics*. 1992;21(4):289–302.
23. Goyal S, EN Pinson, FW Sinden. Simulation of dynamics of interacting rigid bodies including friction II: Software system design and implementation. *Engineering with computers*. 1994;10(3):175–195.
24. Jankowski R. Non□linear viscoelastic modeling of earthquake□induced structural pounding. *Earthquake engineering & structural dynamics*. 2005;34(6):595–611.
25. Muthukumar S, Desroches R. A Hertz contact model with non□linear damping for pounding simulation. *Earthquake engineering & structural dynamics*. 2006;35(7):811–828.
26. Ye K, Li L, Zhu H. A note on the Hertz contact model with nonlinear damping for pounding simulation. *Earthquake Engineering & Structural Dynamics*. 2009;38(9):1135–1142.
27. Andreaus U, Nisticò N. An analytical-numerical model for contact-impact problems: theory and implementation in a two-dimensional distinct element algorithm. *Computer Modeling and Simulation in Engineering*. 1998;3(2):98–110.
28. Andreaus U, M De Angelis. Nonlinear dynamic response of a base-excited SDOF oscillator with double-side unilateral constraints. *Nonlinear Dynamics*. 2016;84(3):1447–1467.
29. Andreaus U, P Casini. Dynamics of friction oscillators excited by a moving base and/or driving force. *Journal of Sound and Vibration*. 2001;245(4):685–699.
30. Andreaus U, Casini P. Forced response of a SDOF friction oscillator colliding with a hysteretic obstacle. *18th Biennial Conference on Mechanical Vibration and Noise*. 2001.
31. Andreaus U, Casini P. Forced motion of friction oscillators limited by a rigid or deformable obstacle. *Mechanics of structures and machines*. 2001;29(2):177–198.
32. Chanda A, A Banerjee, R Das. The Application of the most suitable Impact Model(s) for simulating the Seismic Response of a Straight Bridge under Impact due to Pounding. *International Journal of Scientific and Engineering Research*. 2016;7(2):25–36.
33. Banerjee A, A Chanda, R Das. Historical Origin and Recent Development on Normal Directional Impact Models for Rigid Body Contact Simulation: A Critical Review. *Archives of Computational Methods in Engineering*. 2017;24(2):397–422.
34. Brogliato B. *Nonsmooth mechanics: models, dynamics and control*. Switzerland: Springer Science & Business Media; 2012.
35. Stronge WJ. *Impact mechanics*. Cambridge: Cambridge university press; 2004. 280 p.

36. Wriggers P, TA Laursen. *Computational contact mechanics*. Germany: Springer; 2006.

37. Banerjee A, A Chanda, R Das. Historical Origin and Recent Development on Normal Directional Impact Models for Rigid Body Contact Simulation: A Critical Review. *Archives of Computational Methods in Engineering*. 2017;24(2):397–422.

38. Moreau JJ. *Unilateral Contact and Dry Friction in Finite Freedom Dynamics*. In Nonsmooth Mechanics and Applications, Moreau JJ, Panagiotopoulos PD, Editors. Vienna: Springer; 1988. 82 p.

39. Panagiotopoulos PD. Dynamic and incremental variational inequality principles, differential inclusions and their applications to co-existent phases problems. *Acta Mechanica.* 1981;40(1–2):85–107.

40. Panagiotopoulos PD. Nonconvex energy functions. Hemivariational inequalities and substationarity principles. *Acta Mechanica*. 1983;48(3–4):111–130.

41. Abbas H, DK Paul, PN Godbole, et al. Soft missile impact on rigid targets. *International journal of impact engineering.* 1995;16(5–6):727–737.

42. Glocker C. Set-valued force laws. *Dynamics of non-smooth systems*. 1st ed. Switzerland: Springer Science & Business Media; 2001.

43. Leine R, D Van Campen, CH Glocker. Nonlinear dynamics and modeling of various wooden toys with impact and friction. *Journal of vibration and control*. 2003;9(1–2):25–78.

44. Theodosiou C, S Natsiavas. Dynamics of finite element structural models with multiple unilateral constraints. International *Journal of Non-Linear Mechanics*. 2009;44(4):371–382.

45. Goldsmith W. Impact. Courier Corporation, USA. 2001. 379 p.

46. Pfeiffer F, C Glocker. *Multibody dynamics with unilateral contacts*. Switzerland: Springer Science & Business Media. 2000;421:262.

47. Lemke CE. The dual method of solving the linear programming problem. *Naval Research Logistics Quarterly*. 1954;1(1):36–47.

48. Lemke CE. On complementary pivot theory. Department of Mathematics, Rensselaer Polytechnic Institute, USA. 1967. 76 p.

49. Banerjee A, A Chanda, R Das. Oblique frictional unilateral contacts perceived in curved bridges. *Nonlinear Dynamics.* 2016;85(4):1–25.

Citation: Chanda A, Banerjee A, Das R. Oblique frictional unilateral pounding analysis in two successive curved bridge (s type) segments. *Fluid Mech Res Int.* 2017;1(2):33–43. DOI: 10.15406/fmrij.2017.01.00006